ICAS-88-5.4.4

INVESTIGATION OF FLOW OVER CAVITY-BLUNT BODY COMBINATION AT SUPERSONIC SPEED*

O.H.Rho, D.H.Lee, J.H.Kim and S.J.Kim
Seoul National University
Seoul, Korea

Abstract

In order to understand the essential flow pictures of drag reduction of blunt body in supersonic speed, an investigation has been carried out experimentally and analytically for the two-dimensional cavity flow model simplified from the three-dimensional axisymmetric cavity flow of the conical tip and spiked blunt body combination. The flow for the various two-dimensional cavities have been observed and described systematically, by visualizing the flow from schlieren pictures and by measuring the pressure distribution. The cavity flow field was also analytically computed by solving the two-dimensional Euler equations based on the finite volume method combined with dissipation term and a Runge-Kutta multi-time stepping scheme. The numerical results agree with those of the experiments, particularly the positions of shocks and expansion waves in the cavity. The calculated pressure distributions, however, show some differences from the experimental results and can be improved by making a wake model properly.

I. Introduction

The separated flow, the cavity flow or the flow over the spiked body have many applications in aeronautical engineering problems. They are mainly associated with drag reduction or minimization of maximum heat transfer rate of blunt body in supersonic or hypersonic speed. Many researchers[1,2,3,4], therefore, have been consequently interested in the detailed investigation of the flow composed of separation wake and recompression wake in the cavity formed by the deliberate separation from the extended body. They were, however,mainly concerned with the detailed description of the flow in cavity by measuring the pressure and temperature distributions with parametric changes of the length-to-height ratio , Mach number and Reynolds number. They ,however ,failed in a systematic study of the direct effect on drag reduction of blunt body by considering the various blunt body combinations.

So in order to study a drag reduction of blunt body systematically, the present paper has purposefully chosen the two-dimensional cavity flow model consisted of wedge, cavity and flat-faced body(called the cavity-blunt body combinations at the paper) simply idealized from the three-dimensional axisymmetric cavity flow of the conical tip and spiked blunt body combination. In so doing, analytical as well as experimental study are possible to investigate the essential nature of drag reduction.

II. Experiment

The experiment was conducted at the Seoul National University's supersonic wind tunnel with 20x20 cm test section, room stagnation temperature, variable stagnation pressure with automatic pressure control and continuous flow unit equipped with the two-dimensional fixed nozzle block for M=3. The various test models have been chosen by changing the wedge angle, wedge chord and the cavity length (Fig. 1). The test program for these models was set up to make two type of studies: (a) pressure; (b) phenomenal flow visualization by optical arrangements.

The models was equipped with many pressure holes along the cavity floor, the flat-faced surface and the top surface of the body, which were connected to the recorder through scanivalve and pressure transducer. The pressure distributions were obtained by measuring the pressure along the flat-faced surface of the body as well as the cavity floor by varying systematically the wedge angle, wedge chord and the cavity length, for the three distinct types of cavity flows suggested and defined by Charwat, et al[4]. In doing so, the effect of wedge chord, wegde angle and length were quantitatively investigated.

Fig. 2 & 3 show the effect of variation of wedge angle at fixed wedge chord, by indicating that the increase of wedge angle decreases slightly the pressure level acting on the flat-faced body surface and along the cavity floor. This may be physically explained that change of wedge angle at the fixed wedge chord doesn't alter the formation of separation wake area noticeably.

Figs. 4 & 5 show the effect of variation of wedge chord at the fixed wedge angle. Unlike the case of variation of wedge angle the results indicate the considerable change of pressure level which may be perhaps due to the change of formation of separation wake region.

Figs. 6 show the mean surface pressure on the forward face of the body with increase of the cavity length. It indicate that as the cavity length increases the cavity flow is altering the formation of wake from the open cavity to the closed cavity through the intermediate cavity flow.

Figs.7(a,b), Figs.8(a,b) and Figs.9(a,b) show the spark shadow and schlieren flow phenomenal

*This research was supported by the Korea Science and Engineering Foundation.

visualization of shocks and expansion waves around the cavity flow:

Figs.7(a,b) are the optical photographs of the open cavity flow which is composed of an underexpanded separation wake as a consequence of oblique shocks caused by a flow deflection over the cavity.

Figs.8(a,b) show the pictures of the intermediate cavity flow which is formed by nearly perfectly expanded separation wake where creation of the lowest dynamic pressure is accounted for the minimum pressure drag of the body.

Whereas, Figs. 9(a,b) show the flow phenomenal visualization of the closed cavity which is specifically characterized by separation wake and a relatively strong recompression wake. As a consequence the strong trailing shock is taking place at the free shear layer close to the flow boundary between separation wake and recompression wake where the highest wake pressure is created.

III. Numerical Simulation

The simulated two-dimensional cavity flow was obtained numerically by solving the two-dimensional Euler equations.

The numerical method was based on the finite volume method combined with carefully designed dissipative term and a Runge-Kutta multi-time stepping scheme which was originally proposed by Jameson et al[5]. The detailed computational procedures are given[12]. The computational results are, instead, summarized: The example of the mesh of the two-dimensional cavity flow is shown in Fig. 10(a,b).

Figs. 11(a,b,c,d) are the calculated pressure distributions for the three distinct cavity flow patterns, respectively,and show some differences from the experimental results. It may be explained that the inviscid wake flow calculation doesn't satisfy all the real viscous flow conditions in the cavity. As shown in Fig. 11d, however, the accurate pressure distributions can be obtained from the inviscid flow solutions by proper wake modeling. Fig. 12 shows the calculated pressure distributions along the cavity floor and on the forward face of the body and agrees with the general tendency of the measured pressure distributions. Figs. 13,14,15 and 16 show, respectively, the isobars and Mach number contours for the three cavity flows, which were compared with the shocks, the expansion waves and their positions from the visualization of the optical experiment, and generally agreed well.

IV. Conclusions

In order to understand the essential nature of drag reduction phenomena of the axisymmetric body combination, the experimental and theoretical investigation has been carried out for the simplified two-dimensional model consisted of wedge, cavity and flat-faced blunt body. In so doing, the detailed experiment and the numerical computation can be made with relative easy.

The conclusions are summarized as follows:

(1) The open cavity is entirely composed of an underexpanded separation wake which produces a nearly medium high uniform pressure distributions along the cavity flow and on the flat-faced body surface.

(2) The intermediate cavity is formed by the nearly perfectly expanded wake which gives the lowest pressure distributions for the three cavity flows. The schlieren pictures show no shock in the entire cavity flow. There exist, however, the compression waves eminating from the free shear layer of the recompression wake.

(3) The closed cavity is structurely composed of the overexpanded separation wake and the trailing shock which causes the highest pressure distribution on the forward face of the body.

(4) The inviscid flow solutions computed from the Euler equations can be used to predict the pressure distributions as well as the positions of shocks and expansion waves, by making the wake model properly.

References

1. Charwat, A.F., Roos, J.N., Dewey, F.C., and Hitz, J.A., "An Investigation of Separated Flows" Journal of Aerospace Sci., Vol. 28, No. 6, June 1961.
2. Bogdonoff, S.M. and Vas, I.E., "Preliminary Investigations of Spiked Bodies at Hypersonic Speeds" Journal of Aerospace Sci., Vol. 26, No. 2,Feb. 1959, pp. 65 - 74.
3. Crawford, D.H., "Investigation of the Flow over a Spiked-Nose Hemisphere-Cylinder at a Mach No. of 6.8", NASA TN D-118, Dec. 1959.
4. Bestall, D. and Turner, J., "The Effect of a Spike Protruding in front of a Bluff Body at Supersonic Speeds", ARC Tech. Rept. R and M 3007, Jan. 1952.
5. A. Jameson, W. Schmidt, E. Turkel, "Numerical Solution of the Euler Equations by Finite Volume Methods using Runge-Kutta Time-Stepping Schemes" AIAA Paper 81-1259.
6. T.H. Pulliam, "Artificial Dissipation Models for the Euler Equations" AIAA J., Vol. 24, No. 12, pp. 1931-1949, 1986.
7. A. Jameson and D. Mavriplis, "Finite Volume Solution of the Two-Dim. Euler Equations on a Regular Triangular Mesh" AIAA J., Vol. 24, No. 4, 1986.
8. J. Pike and Roe P.L., "Accelerated Convergence of Jameson's Finite-Volume Euler Scheme using Van Der Houwen Integrators", Computers & Fluids, Vol. 13, No. 2, pp. 223-236, 1985.
9. J.L. Thomas and M.D. Salas, "Far-Field Boundary Conditions For Transonic Lifting Solutions to the Euler Equations" AIAA J., Vol.

24, No. 7, pp. 1074-1080, 1986.
10. D. Kwak, "Nonreflecting Far-Field Boundary Conditions For Unsteady Transonic Flow Computing" AIAA J., Vol. 19, No. 11, pp. 1401-1407,1981.
11. J.F. Thompson, "Grid Generation Techniques in Computional Fluid Dynamics" AIAA J., Vol. 22, No. 11, pp. 1505-1523, 1984.
12. O.H. Rho, D.H. Lee, J.H. Kim and S.J. Kim, " Investigation of Flow over Cavity-Blunt Body Combination at Supersonic Speed" Seoul National University Technical Report #88-3, 1988

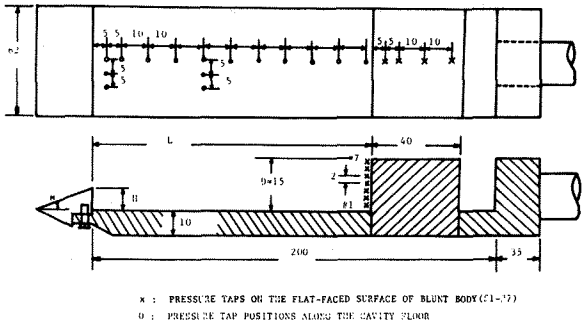

WEDGE MODEL	1	2	3	4	5	6	7	8	9
φ (DEG.)	12.4	10.2	8	6.8	9.6	18.3	9.2	9.2	9.2
H(mm)	7	7	7	3.5	5	9.9	4	5	6

Fig.1 Diagram of Two-Dimensional Cavity Model

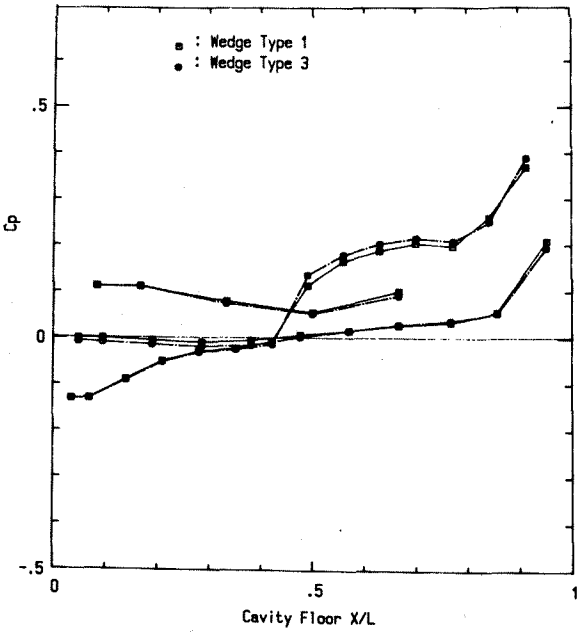

Fig.2 The Effect of Variation of Wedge Angle on Pressure Distribution along the Cavity Floor

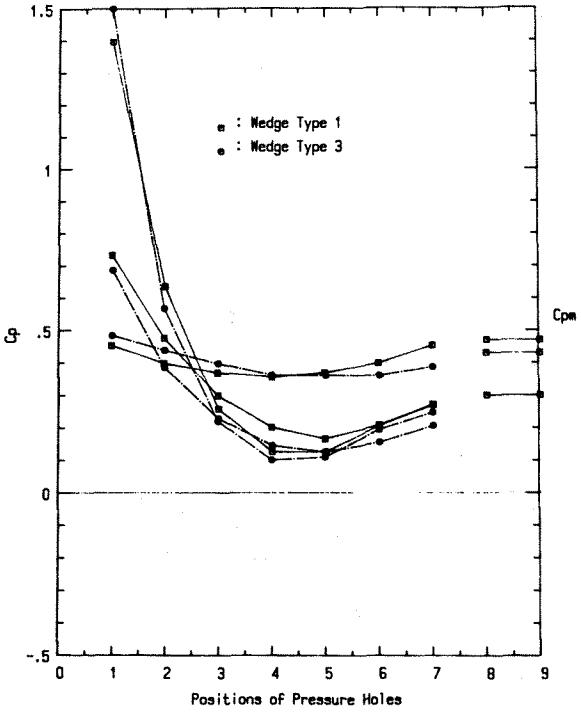

Fig.3 The Effect of Variation of Wedge Angle on Pressure Distribution on the Flat-Faced Body Surface

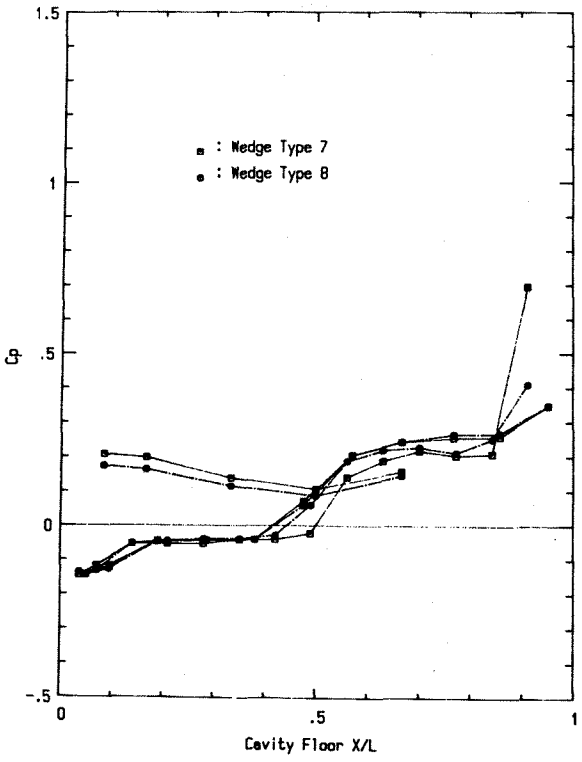

Fig.4 The Effect of Variation of Wedge Chord on Pressure Distribution along the Cavity Floor

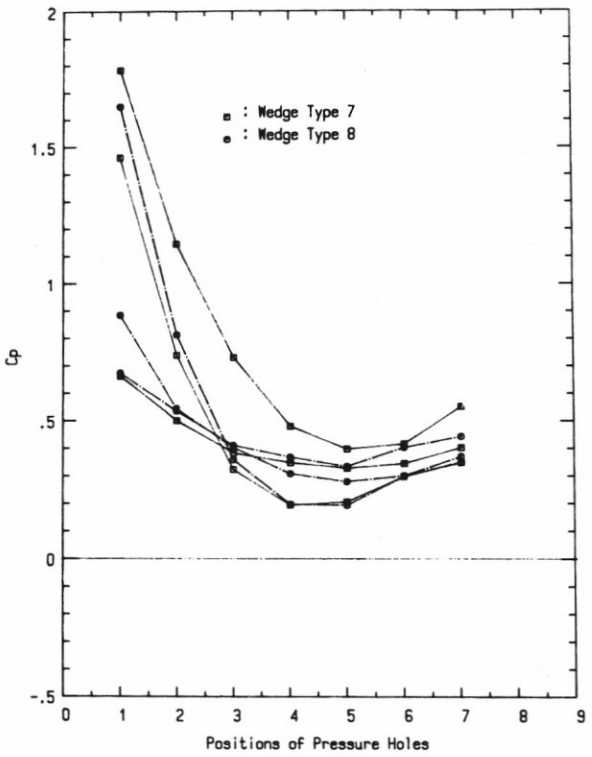

Fig.5 The Effect of Variation of Wedge Chord on Pressure Distribution on the Flat-Faced B -ody Surface

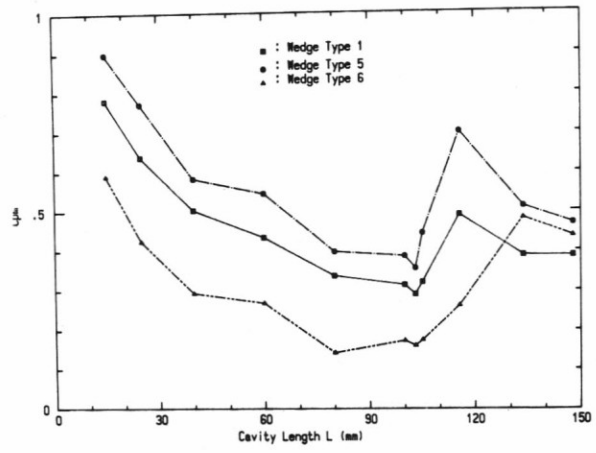

Fig.6 Mean Pressure on Flat-Faced Body Surface

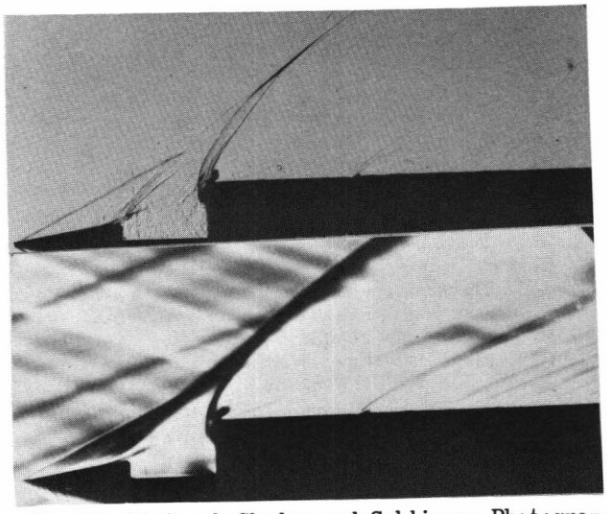

Fig.7(a,b) Spark Shadow and Schlieren Photographs of the Open Cavity Flow

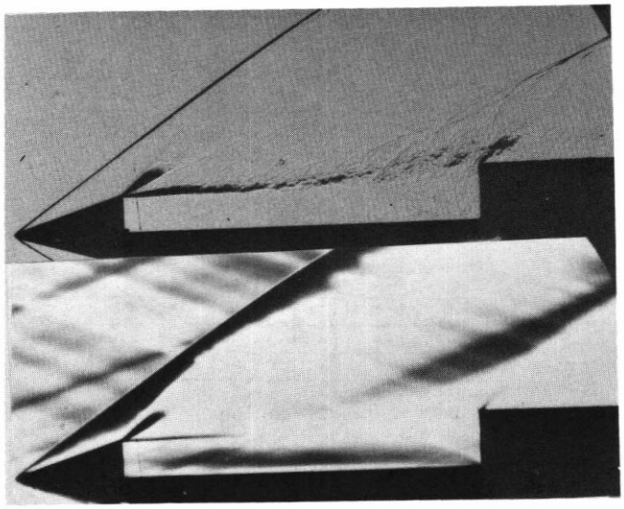

Fig.8(a,b) Spark Shadow and Schlieren Photographs of the Intermediate Cavity Flow

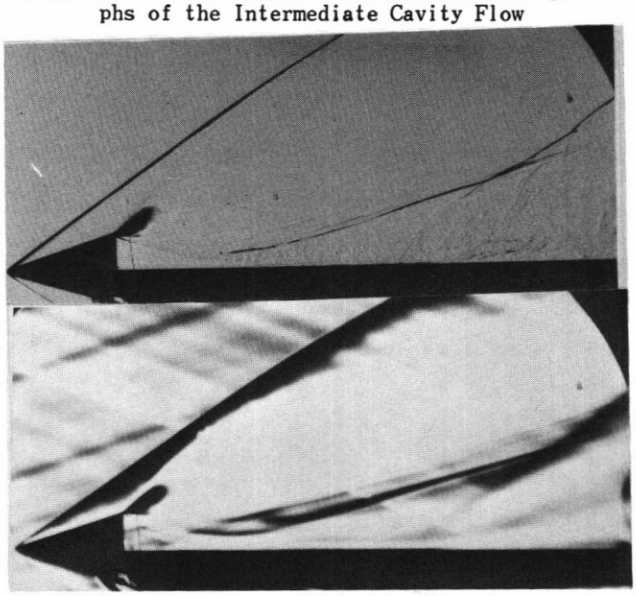

Fig.9(a,b) Spark Shadow and Schlieren Photographs of the Closed Cavity Flow

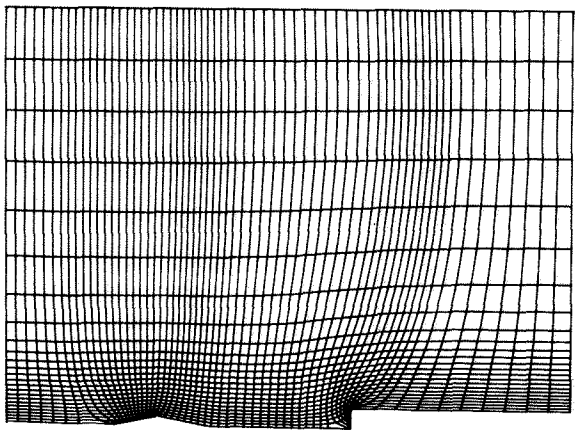

Fig.10 Mesh of Two-Dimensional Cavity with Modified Wake

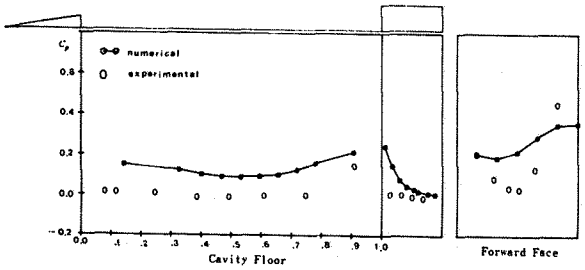

(a) Open Type

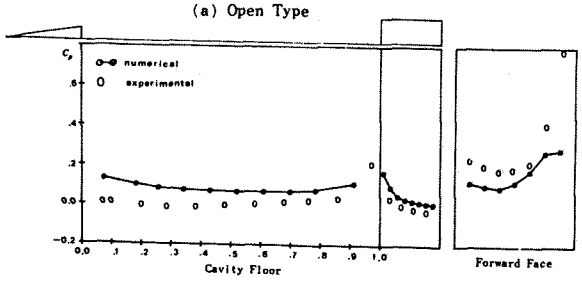

(b) Intermediate Type

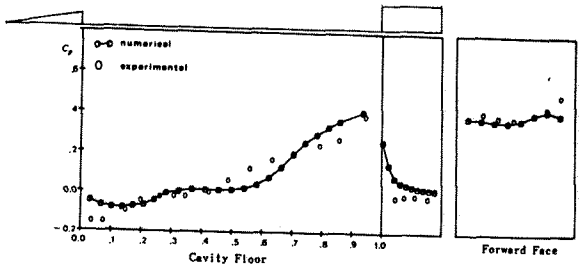

(c) Wake Modelling

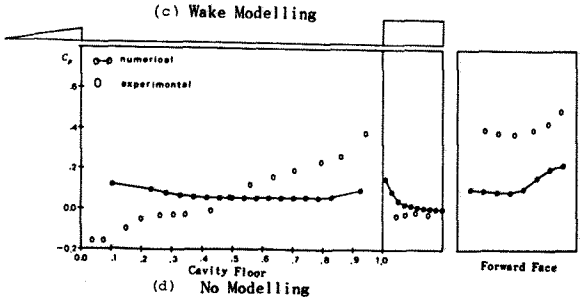

(d) No Modelling

Fig.11(a,b,c,d) Computational Pressure Distributions and Comparisons with Experimental Data, for Three Cavity Flows

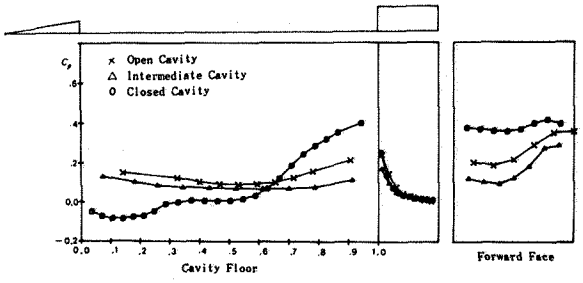

Fig.12 Computed Pressure Distributions for Three Cavity Flow Patterns. The Computed Results, However, Agree with the General Tendency of Experimental Pressure Distributions.

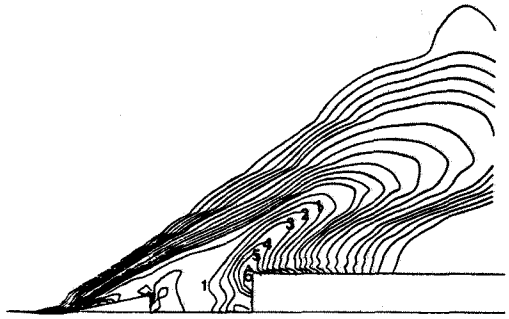

(a) Isobar Contour

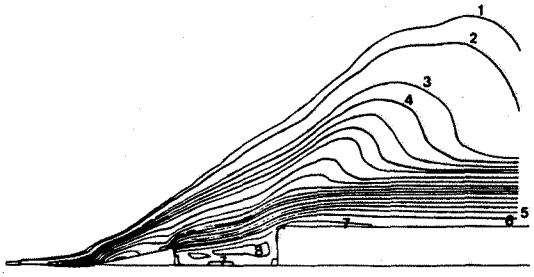

(b) Isomach Contour

Open Case :
Mach 3.0 , Mesh 42 X 16 , Type 1 , L/D 2.67

Fig.13(a,b) Computed Equal Density and Mach Number Contours for the Open Cavity Flow

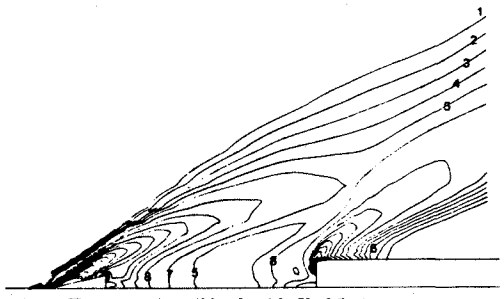

(a) Type : 1 (Mesh 48 X 25)

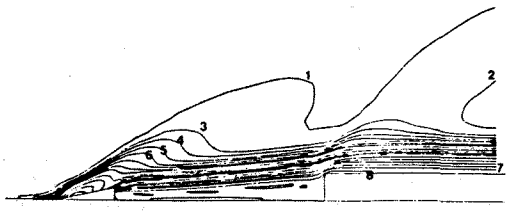

(b) Type : 1 (Mesh 48 X 25)

Isomach - Intermediate Case

Fig.14(a,b) Computed Equal Density and Mach Number Contours for the Intermediate Cavity Flow, M=3
(a) Isobar Contours, (b) Isomach number Contours

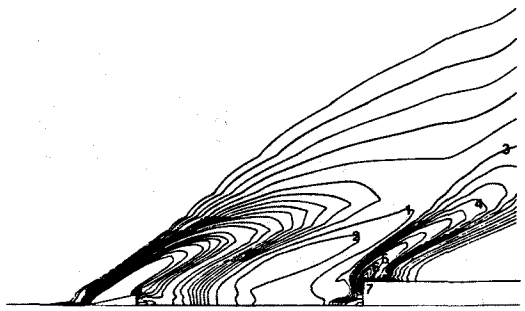

(a) Type : 1

Isobar - Closed Case : (Mach 3.0 , Mesh 64 X 24)

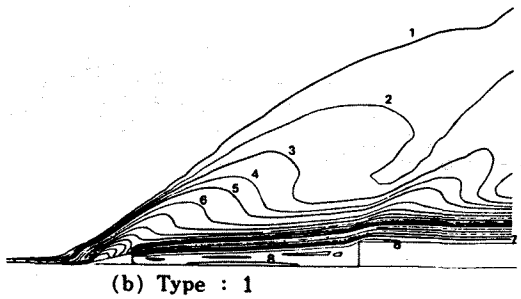

(b) Type : 1

Isomach - Closed Case : (Mach 3.0 , Mesh 64 X 24)

Fig.15(a,b) Computed Isobar and Isomach Number Contours for the Closed Cavity

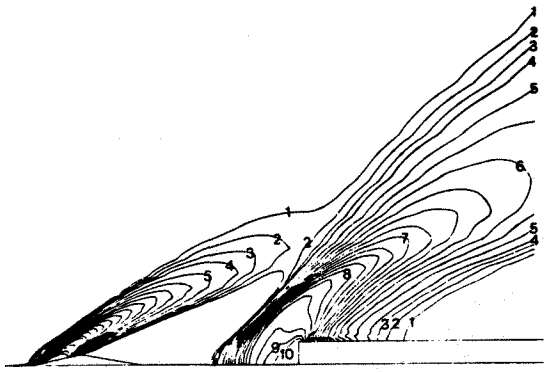

(a) Isobar Contour

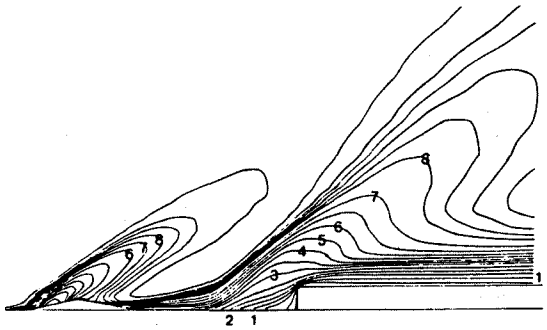

(b) Isomach Contour

Wake Modelling - Contour Type 1 , β 80°

Fig.16(a,b) Computed Isobar and Isomach Number Contours for the Closed Cavity with Wake Modelling